JOURNAL OF AIRCRAFT
Vol. 35, No. 6, November–December 1998

Flutter Control of Wing Boxes Using Piezoelectric Actuators

Edwin E. Forster*
Purdue University, West Lafayette, Indiana 47907
and
Henry T. Y. Yang†
University of California, Santa Barbara, Santa Barbara, California 93106

This paper examines the use of piezoelectric actuators to control supersonic flutter of wing boxes. Aluminum built-up wing boxes are used as examples to analyze the free-vibration, aeroelastic, and control concepts associated with flutter control. Finite elements are used to calculate deflections caused by input forces, the member stresses and strains, natural frequencies, and mode shapes. Linear strip theory with steady aerodynamics is applied to find the frequency coalescence of modes indicating flutter. The variables of interest are the skin, web, and rib thicknesses associated with torsional rigidity, and the spar cap and vertical post areas associated with bending rigidity. Piezoelectric actuators are implemented in a configuration that generates torsional control of the wing box. Pole assignment concepts are applied to change the free-vibration frequencies. A parametric study changing the free-vibration frequencies using piezoelectric actuators is conducted to determine which thicknesses of skins, webs, and ribs will meet a specified flutter requirement. The addition of piezoelectric actuators will allow the flutter requirements to be met at smaller thicknesses of skins, webs, and ribs so that the overall weight of the wing box, including actuators, is decreased.

Introduction

FLUTTER is defined as the instability associated with increasing amplitudes of oscillation because of the interaction of modes with inertial and aerodynamic coupling. This aeroelastic instability is a concern for aircraft and wing designers. Traditionally, control of this instability has been primarily accomplished using conventional lift control surfaces such as ailerons. More recently, advanced control devices such as strain actuators have been proposed to control flutter.

Active flutter suppression uses control surfaces with classic control techniques to change the aeroelastic behavior of a wing. The field of aeroservoelasticity has been explored by many investigators, such as Zeiler and Weisshaar,[1] and Karpel.[2] Zeiler and Weisshaar presented the problem of integrated aeroservoelastic tailoring using a four-degree-of-freedom aeroelastic model. Karpel analytically developed the flutter and stability margin derivatives with respect to aeroservoelastic design and utilized a mathematical model of the active flexible wing (AFW) wind-tunnel model as an example. Among those who summarized the works on aeroservoelasticity, Noll[3] described the work of the aeroservoelasticity branch of the NASA Langley Research Center on the active flexible wing program that demonstrated a 20% increase in flutter dynamic pressure in wind-tunnel tests. These examples show that control surfaces were successfully utilized for flutter suppression.

Flutter control utilizing strain actuators requires both sensing and adaptive characteristics. Wada et al.[4] propose that sensory structures possess sensors for the determination of the system states and characteristics, whereas adaptive structures possess actuators to change the system states and characteristics. An adaptive material that has the property of piezoelectricity may be suited for control applications. A piezoelectric material produces a charge when stress is applied. Conversely, these materials can produce a strain when an electric field is applied. Examples of piezoelectrics include lead zirconate titanate (PZT) and polyvinylidine fluoride (PVDF). Because of their dual nature, piezoelectrics can both act as sensors and actuators.

Piezoelectric actuators have been used to change the shape of host structures. Barrett[5] showed that directionally attaching an in-plane orthotropic actuator restricted longitudinal displacements, whereas the lateral displacements had little restriction. With this method, a host structure consisting of an isotropic material could be twisted using a piezoceramic, such as PZT. Abdul-Wahed and Weisshaar[6] showed that cantilever beams with a skewed PZT actuator array produced deflection and twist, and skewed axis PVDF actuator arrays created twist only. De Luis and Crawley[7] showed that the flexible modes of a composite beam could be controlled using piezoelectric. These examples illustrate the effectiveness of piezoelectric materials as actuators.

Modifying the aeroelastic behavior of host structures has attracted special attention for advanced applications of piezoelectric materials. Ehlers and Weisshaar[8] examined the use of piezoelectrics to enhance the static aeroelastic behavior of composite wings. Lazarus et al.[9] examined the feasibility of using adaptive materials for static aeroelastic control of a box wing. The trade studies performed showed that better control authority with decreased weight could be obtained for some wing configurations. Lazarus et al.[10] conducted a typical section analysis to determine the effectiveness of torsion and bending strain actuation vs leading- and trailing-edge flap control. Control cost comparisons indicated that, for the two-degree-of-freedom section, one bending and one torsion actuator produce the best combination. These examples illustrate the potential utility of piezoelectric actuators in aeroelastic applications.

In this paper, a feasibility analysis for flutter control is shown for the example of a fully built-up wing box with piezoelectric actuators. The wing box provides a model of a three-dimensional built-up structure for which attachment of strain actuators may be a meaningful subject of research with potential for flutter control applications, yet simple enough for parametric trade studies to be performed. A piezoelectric ac-

Received Feb. 28, 1996; revision received Feb. 16, 1998; accepted for publication June 24, 1998.

*Graduate Student, School of Aeronautics and Astronautics.
†Professor of Mechanical and Environmental Engineering and Chancellor. Fellow AIAA.

tuator configuration that controls the twist of the wing box is implemented to change the free-vibration frequencies and modes, thus, controlling flutter speed. The effectiveness of piezoelectric actuation to meet a specified flutter requirement is demonstrated in the parametric variation of thicknesses of skins, webs, and ribs. These parametric studies show that the weight of the wing box can be decreased by adding piezoelectric actuators to meet the flutter requirement at smaller thicknesses of skins, webs, and ribs.

Model Configuration

An example of the wing box is depicted in Fig. 1. It is assumed to be a six-bay model. The skins are modeled using 12 eight-degree-of-freedom quadrilateral membrane elements. The webs and ribs are modeled using 18 eight-degree-of-freedom shear panel elements, and the spar caps and vertical posts are modeled using 36 two-degree-of-freedom bar elements. The finite element formulations are based on those presented by Venkayya and Tischler.[11] It is noted that wing box structures for supersonic aircraft are less likely to behave as idealized structures as that by Megson,[12] in which stringers and spar caps carry bending loads and skins and webs carry shear loads. In supersonic aircraft, skins are thicker and airfoils have lower airfoil thickness to chord ratios. However, in this study, the emphasis is on the preliminary investigation of the potential beneficial effect of using piezoelectric materials to help control flutter. The structures and the aerodynamic flows are modeled in the simplest possible ways for straightforward computer simulations, yet the results can provide some insights to the physical behavior and also some meanings from the approximate trade data because of the effect of piezoelectric actuators. Thus, the built-up box structures are simply modeled as those previously described, and the aerodynamics is simplified as supersonic based on the two-dimensional linear strip theory.

The six-bay wing box is the same model used by Bowman et al.,[13] which is a modified version of the three-bay wing box optimized for flutter by Rudisill and Bhatia.[14,15] Striz and Venkayya[16] demonstrated that the use of membrane elements for webs and ribs overpredicts the stiffness of a wing. Here, the aspect ratio of 15 for the webs was too high, even for dynamic analysis. The extensive static, dynamic, and aeroelastic studies performed on this wing box structure allowed comparison of the results from this study.

The finite element variables of thickness and cross-sectional area are assumed to be uniform over the span of the wing box. Furthermore, the skin, web, and rib members, which are associated with torsional rigidity, are assumed to have the same thicknesses, and the spar cap and vertical post members, which are associated with bending rigidity, are assumed to have the same cross-sectional areas. The symmetry of the wing box always locates the shear center in the center of the wing box. The uniform wing without nonstructural masses has the c.m. at the same location as the shear center. The addition of nonstructural mass, say, equal to the structural mass, along the rear spar will locate the center of mass midway between the rear spar and the shear center.

The location of the wing box in the aerodynamic shell is shown in Fig. 2. The shell is assumed to not carry any structural stresses, and all aerodynamic forces are directly translated to the spars. For subsonic and supersonic flight, the aerodynamic center (A.C.) is assumed to be located at the quarter-

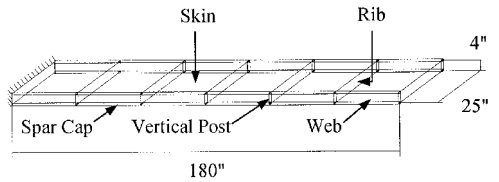

Fig. 1 Dimensions and member identification of built-up aluminum wing box.

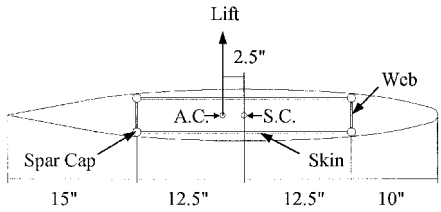

Fig. 2 Cross section of wing.

chord and the half-chord, respectively. For subsonic flow, the aerodynamic center is in front of the shear center (S.C.), whereas for supersonic flow the aerodynamic center is aft of the shear center.

The two-dimensional aerodynamic grid is attached to the structure with six aerodynamic strips: the edges are lined up with the ribs of the structure. The ribs and aerodynamic strips are assumed to stay perpendicular to the span as the wing is swept. A first-order, high Mach number approximation is used for the aerodynamics.[17] The aerodynamic loads acting on a strip are assumed to be functions of the deflections of only that strip. The lift is given as

$$L = \tfrac{1}{2}\rho V_n^2 S C_{L_\alpha} \alpha_{\text{eff}} \tag{1}$$

where V_n is the chordwise component of the actual airspeed. The air density, ρ, is dependent on the altitude, and the lift curve slope, C_{L_α}, is dependent on Mach number. The effective angle of attack is the angle of the strip with respect to V_n

$$\alpha_{\text{eff}} = \alpha - \Gamma \tan \Lambda \tag{2}$$

where α is the chordwise rotation, Γ is the spanwise rotation, and Λ is the sweep of the section with respect to the free-stream.

A piezoelectric material produces a three-dimensional state of strain when an electric field is applied. For the case of stress-free expansion, the relation between strains and electric fields is

$$\{\epsilon\} = [d]\{E\} \tag{3}$$

where $\{\epsilon\}$ is the vector of strains, $[d]$ is the matrix of piezoelectric strain coefficients, and $\{E\}$ is the vector of applied electric fields. PZT is a transversely isotropic material, with the plane of the wafer being the isotropic plane. PVDF is an isotropic material with orthotropic electrically induced in-plane strains. The magnitude of the charge coefficient directly specifies the amount of unrestricted strain that can be achieved for a particular direction. The charge coefficients of PVDF are larger than those of PZT. For a piezoceramic, such as PZT, the shear charge coefficients (d_{35}) are the largest, the charge coefficient in the poling direction (d_{33}) is second largest, and the charge coefficients in the plane perpendicular to the poling direction (d_{31}, d_{32}) are the smallest in magnitude. Most current applications utilize this last type of configuration.

A comparison of material properties of aluminum and piezoelectric materials appears in Table 1. PZT has the approximate modulus of aluminum with the density of steel which, along with its actuation coefficient, makes it a potentially good actuator. PVDF has a much smaller modulus and it is more suitable for a sensing medium. PZT has the inherent problem of brittleness, as do all ceramics, indicated by its maximum strain, $\varepsilon_{\max} = 300\ \mu\varepsilon$. Sheets are available in 0.005, 0.0075, and 0.010 in. (0.013, 0.019, and 0.025 cm) thicknesses.[18] For the nominal thickness of 0.0075 in., the maximum voltage applied is 40–50 V in the poling direction, relating to the maximum strain.

In this study, a standard axial force member is used to model the piezoelectric actuator. The actuator configuration is shown

Table 1 Comparison of material properties of aluminum and piezoelectric materials

Material properties	Aluminum	PZT	PVDF
Modulus of elasticity, 10^6 psi	10.0	9.135	0.29
Density, lb/in.^{3}	0.1	0.275	0.064
Poisson's ratio	0.3	0.35	0.3
Tensile strength, ksi	65.0	9.135	4.5–8.0
Compressive strength, ksi	65.0	75.4	——
Activation coefficient, d_{31}, m/V	——	-166×10^{-12}	23×10^{-12}

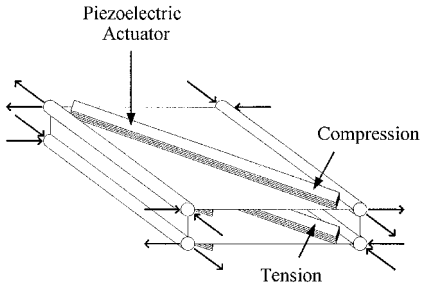

Fig. 3 Piezoelectric actuator configuration.

in Fig. 3. Arrows indicate the resultant force on the wing box caused by activation of the piezoelectric actuators. The piezoelectric actuator under compression pushes the host structure outward, whereas the actuator in tension pulls the host structure inward. The upper and lower skins each have an actuator in compression and tension for a positive electric field. A negative electric field reverses the actions of both members. Twisting of the wing box is caused by shearing the upper and lower skins in opposite directions. The lateral strain of the piezoelectric actuators is ignored because the actuators are assumed directional. For PZT actuators, this simplification of the actuator attachment follows Barrett's[5] work to directionally attach PZT elements to host structures. Axial force members are used because of the high aspect ratio of the actuator elements. All strips are assumed to be 1.0 in. (2.5 cm) wide with height equal to the number of layers multiplied by the nominal thickness 0.005 in. Buckling of the actuators is neglected because the elements are bonded to the skin surface.

The axial force member will produce a strain dependent on the electrical and mechanical loading

$$\varepsilon = \varepsilon^M + \varepsilon^E \tag{4}$$

where the superscript M indicates mechanical, and the superscript E indicates electrical. The finite element method uses a simple superposition of electrical forces and forces in the member caused by the induced displacements to find the resultant forces in the member, as outlined in Chapter 5 of the text by Yang.[19]

Structural Dynamics and Control Analysis

The equations of motion for the wing box are

$$[M]\{\ddot{\boldsymbol{X}}\} + [K]\{\boldsymbol{X}\} = \{\boldsymbol{F}(t)\} \tag{5}$$

where $[M]$ is the mass matrix, $[K]$ is the stiffness matrix, $\{\boldsymbol{X}\}$ is the vector of nodal displacements, $\{\ddot{\boldsymbol{X}}\}$ is the vector of nodal accelerations, and $\{\boldsymbol{F}(t)\}$ is the vector of forcing functions. The mass matrix is assembled using lumped mass formulation for membrane, shear panel, and bar elements. It is noted that the choice between the formulations using lumped masses and consistent masses has been of interest to the finite element analysts. For the case of a two degree-of-freedom bar element in axial vibration, which is used for modeling spar caps and vertical posts, it has been shown in Chapter 7 of the text by Yang,[19] that for a one-element solution for the first natural frequency, the error is +10.3% for the consistent mass formulation and −10.0% for the lumped mass formulation. Both errors reduce to +2.56 and −2.53%, respectively, at the two-element level. For three-element modelings, both errors are close to ±1%. For the membrane elements modeling skins, webs, and ribs, a similar dilemma in choosing between consistent and lumped masses is observed. However, for the purpose of simple modeling with interests primarily in approximating the general trends in flutter behaviors, either lumped or consistent mass modeling would give results with about the same level of satisfaction. The lumped mass modeling is thus used for no better or worse reason than using the consistent mass modeling.

For the case of free vibration, the equations reduce to an eigenvalue problem

$$[[K] - \omega^2[M]]\{\boldsymbol{U}\} = \{\boldsymbol{0}\} \tag{6}$$

where ω is the natural frequency, and $\{\boldsymbol{U}\}$ is the mode shape.

In the case of steady aerodynamics, the vector of forcing functions is replaced by

$$\{\boldsymbol{F}(t)\} = [A_K]\{\boldsymbol{X}\} \tag{7}$$

where $[A_K]$ is the aerodynamic stiffness matrix.

The equations of motion are simplified using the information of the free vibration natural frequencies and mode shapes. By substituting into the equation

$$\{\boldsymbol{X}\} = [\Phi]\{\boldsymbol{Q}\} \tag{8}$$

where $[\Phi]$ is the matrix of orthonormal modes, and premultiplying the equation by $[\Phi]^T$, the equations of motion become

$$[\Phi]^T[M][\Phi]\{\ddot{\boldsymbol{Q}}\} + [\Phi]^T[K][\Phi]\{\boldsymbol{Q}\} = [\Phi]^T[A_K][\Phi]\{\boldsymbol{Q}\} \tag{9}$$

This equation is simplified by substituting back the relations for orthonormal modes and transforming into state-space form

$$\begin{Bmatrix} \dot{\boldsymbol{Q}} \\ \ddot{\boldsymbol{Q}} \end{Bmatrix} = \begin{bmatrix} 0 & I \\ -[\Omega^2] + [\bar{A}_K] & 0 \end{bmatrix} \begin{Bmatrix} \boldsymbol{Q} \\ \dot{\boldsymbol{Q}} \end{Bmatrix} \tag{10}$$

where $[\bar{A}_K] = [\Phi]^T[A_K][\Phi]$ is the modal aerodynamic influence coefficient matrix, and $[\Omega^2]$ is the diagonal matrix of natural frequencies. Flutter for this formulation occurs when frequencies coalesce on the imaginary axis and then produce a 90-deg phase shift indicative of increasing amplitude behavior. Divergence occurs when the frequency of oscillation is zero and there is no damping in the system, i.e., when the root loci pass through the imaginary axis. These dynamic and static instabilities can be seen in Fig. 4. For the case when the first three modes only are used for reduction, the characteristic polynomial is

$$\lambda^6 + p\lambda^4 + q\lambda^2 + r = 0 \tag{11}$$

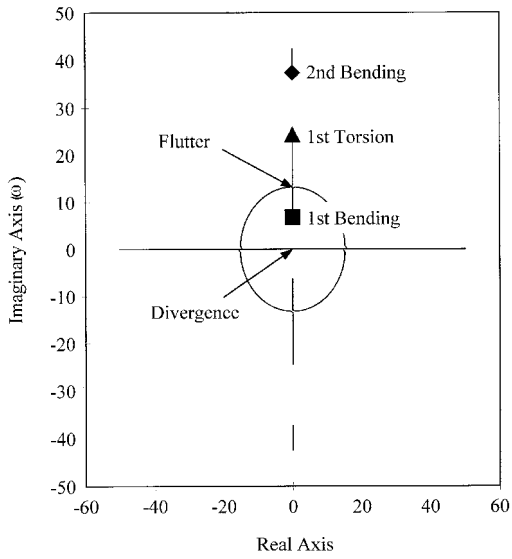

Fig. 4 Velocity root locus representation of flutter and divergence speeds.

where the values for the coefficients are

$$p = -(a_{11} - \omega_1^2) - (a_{22} - \omega_2^2) - (a_{33} - \omega_3^2) \tag{12}$$

$$q = (a_{11} - \omega_1^2)(a_{22} - \omega_2^2) + (a_{22} - \omega_2^2)(a_{33} - \omega_3^2) + (a_{33} - \omega_3^2)(a_{11} - \omega_1^2) - a_{12}a_{21} - a_{23}a_{32} - a_{31}a_{13} \tag{13}$$

$$r = -|[\bar{A}] - [\Omega^2]| \tag{14}$$

where a_{ij} denote the coefficients of the modal aerodynamic stiffness matrix. The characteristic equation indicates a highly coupled system caused by the aerodynamic terms. Flutter occurs when there is a multiplicity of the roots of the characteristic equation, the procedure for finding the roots is standardized if p, q, and r are real.[20]

The addition of forces caused by the piezoelectric actuators into the equations of motion is accomplished by adding input forces

$$\{\boldsymbol{b}\} = \begin{Bmatrix} 0 \\ [\Phi]^T\{\boldsymbol{P}\} \end{Bmatrix} \tag{15}$$

where $\{\boldsymbol{P}\}$ is the matrix of forces per unit input, into the state-space form

$$\{\dot{\boldsymbol{x}}\} = [A]\{\boldsymbol{x}\} + \{\boldsymbol{b}\}\boldsymbol{u} \tag{16}$$

where $\boldsymbol{u}$ is the vector of strain (or voltage) input. For the present problem it is assumed that only one input is used, so $\boldsymbol{u}$ is a scalar and $\{\boldsymbol{b}\}$ is a vector of forces per unit input. Control for this problem is the feedback

$$u = \lfloor \boldsymbol{G} \rfloor \{\boldsymbol{x}\} \tag{17}$$

where $\lfloor \boldsymbol{G} \rfloor$ is the row vector of modal gains, which changes the state-space form to the following:

$$\begin{Bmatrix} \dot{\boldsymbol{Q}} \\ \ddot{\boldsymbol{Q}} \end{Bmatrix} = \begin{bmatrix} 0 & I \\ [\Omega^2] + [\bar{A}_K] + [\Phi]^T\{P\}\lfloor G \rfloor & 0 \end{bmatrix} \begin{Bmatrix} \boldsymbol{Q} \\ \dot{\boldsymbol{Q}} \end{Bmatrix} \tag{18}$$

The determination of the gain is dependent on the closed-loop poles desired. Pole assignment is the method of specifying the eigenvalue location. Skelton[21] remarks that "eigenvalue location is rarely an adequate statement of control objectives, since the eigenvectors, the zeros, the cost function, and the output correlation are all ignored in this control objective." In this study, the free-vibration frequencies of specified modes are modified, so that the zeros, cost function, and output correlation are not factors in the determination of the gain. The understanding of modal behavior with increasing airspeed indicates that eigenvectors will allow the implementation of this control concept. Thus, pole assignment seems an adequate method for determining the trends of flutter for this parametric study.

To change the free-vibration frequency of one mode, for example, the second-mode frequency, ω_2 to $\hat{\omega}_2$ requires the feedback

$$\lfloor G \rfloor = \left\lfloor 0 \; \frac{\omega_2^2 - \hat{\omega}_2^2}{\{U_2\}^T\{P\}} \; 0 \; 0 \; 0 \right\rfloor \tag{19}$$

The characteristic polynomial of the full equations of motion has been changed by the addition of control coupled terms to the matrix. The coefficients of the new characteristic polynomial are

$$\hat{p} = p \tag{20}$$

$$\hat{q} = q - \left(a_{21} \frac{\{U_1\}^T\{P\}}{\{U_2\}^T\{P\}} + a_{23} \frac{\{U_3\}^T\{P\}}{\{U_2\}^T\{P\}} \right) (\omega_2^2 - \Omega_2^2) \tag{21}$$

$$\hat{r} = r + \left(a_{23} \left(a_{31} \frac{\{U_1\}^T\{P\}}{\{U_2\}^T\{P\}} - (a_{11} - \omega_1^2) \frac{\{U_3\}^T\{P\}}{\{U_2\}^T\{P\}} \right) + a_{21} \left(a_{13} \frac{\{U_3\}^T\{P\}}{\{U_2\}^T\{P\}} - (a_{33} - \omega_3^2) \frac{\{U_1\}^T\{P\}}{\{U_2\}^T\{P\}} \right) \right) (\omega_2^2 - \Omega_2^2) \tag{22}$$

The characteristic equation is highly coupled because of both aerodynamic and control terms. A special case, the inertially uncoupled system, has the terms $\{\boldsymbol{U}_1\}^T\{\boldsymbol{P}\} = \{\boldsymbol{U}_3\}^T\{\boldsymbol{P}\} = 0$; consequently, the change in frequency of the torsion root does not affect the aerodynamic modal behavior of the other modes. The frequencies of all the modes of the coupled system can be changed. Changing the first or third mode will permutate the coefficients in Eqs. (21) and (22). The aerodynamic modal behavior can be modified by changing any one or more modal frequencies in the coupled system.

Illustrative Examples

To illustrate the present formulations and computational procedures for the flutter analysis and control of wing box structures in supersonic flow, a series of illustrative examples have been analyzed with results evaluated numerically and interpreted physically. A built-up wing box, rather than beam or plate representations of a wing structure, has been selected to ensure that the actuator placement is addressed for a relatively more realistic representation. The six-bay wing box model has been selected as it may sufficiently provide for reasonable flutter velocity determination, yet provide the necessary simplicity for parametric trend evaluations. The methodology used and the insight gained can be applied to more complex wings. In fact, for this study, wing boxes of four and seven bays were also analyzed, although not to the extent of parametric studies. It was felt that a wing box of six bays can characterize the dual purpose of accuracy and simplicity reasonably well.

Free-Vibration Analyses of Wing Box Models

The free-vibration natural frequencies and mode shapes were first obtained for a three-bay wing box model and compared with those values presented by Striz and Venkayya.[16] The variables used for this comparison were the same as those given in Ref. 18: skin and rib thickness of 0.04 in. (0.10 cm), web thickness of 0.08 in. (0.20 cm), and spar cap and vertical post area of 2.0 in.^{2} (12.9 cm^2); good agreement was found.[22] The first six natural frequencies and mode shapes for a six-

bay wing box model were then computed and are presented in Fig. 5. As compared with the results for the three-bay model, the frequencies and mode shapes for the first three modes are in good agreement, but not in the three other higher modes. The three-bay model did not have enough degrees of freedom to accurately model the second, third, and third torsion modes.

Utilizing a lumped mass matrix formulation is sufficient for determining the trends of free-vibration frequencies for design variables. To study the trends of the free-vibration behavior, the thicknesses of the skins, webs, and ribs were varied with the cross-sectional areas of the spar caps and vertical posts held at a constant value of 1.0 in.^{2} (6.5 cm^2). These trends were studied for a wing box with and without attached nonstructural masses. Adding nonstructural mass to the rear spar changes the modal behavior of the wing box. The torsion and bending modes have been coupled, particularly the first torsion and second bending modes. As an example, it was assumed that adding the nonstructural masses equaled the mass of the original box structure. By doing so, the c.m. is always kept midway between the shear center and the rear spar. The natural frequencies of the first three modes for both cases are presented in Fig. 6, for easy comparison.

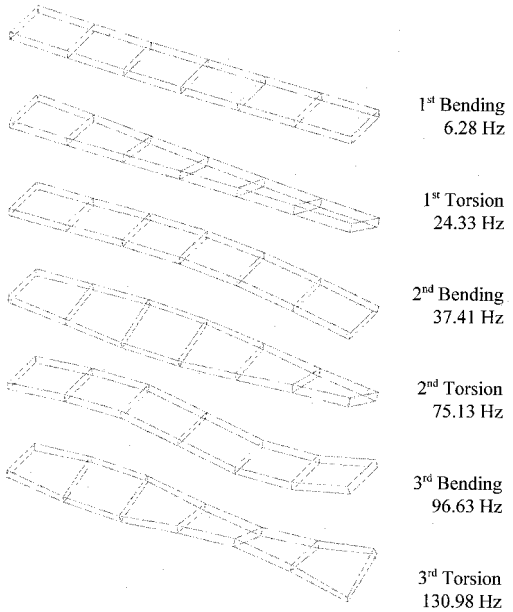

Fig. 5 Natural frequencies and mode shapes for first six modes of six-bay wing box.

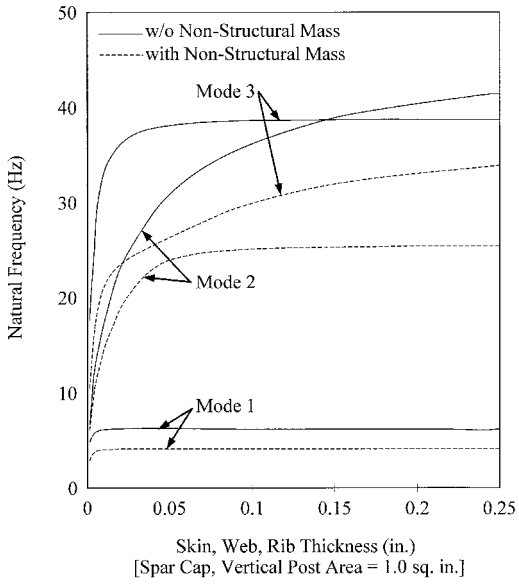

Fig. 6 Effect of skin, web, and rib thickness on first three natural frequencies of wing box with and without nonstructural masses.

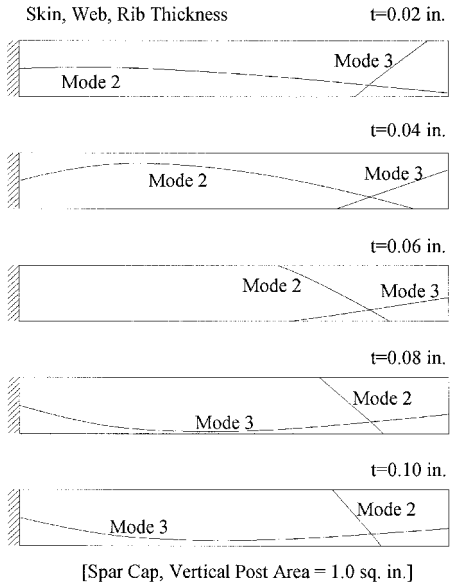

Fig. 7 Effect of skin, web, and rib thickness on nodal line representations for second and third mode shapes of wing box with nonstructural masses.

For the wing box without nonstructural masses, the first torsion and second bending frequencies cross at a thickness of 0.130 in. (0.320 cm). All three frequencies increase rapidly at thickness values less than, say, 0.010 in. (0.025 cm), but both bending mode natural frequencies level off. For the present class of wing boxes, the increase in bending rigidity caused by the increase in web and skin thickness is canceled by the increase in masses because of the increase in all three thicknesses. The torsion frequency increases with the thicknesses of the skins, webs, and ribs. Obviously, the effect of stiffness increases faster than that of the masses.

For the wing box with attached nonstructural masses, the trends of the first three modes are similar to those of the wing box without nonstructural masses for the lower thickness values, say, below 0.02 in. (0.05 cm). From thickness values of 0.04–0.06 in. (0.10–0.15 cm) the trends are that the second frequency, originally of the first torsional mode, levels off and becomes that of a second bending mode, whereas the third frequency, originally of the second bending mode, keeps increasing and becomes that of a torsional mode. This phenomenon of switching the first torsional and second bending mode is explained in Fig. 7 by plotting the migrations of the nodal lines of the two modes as the member thicknesses increase from 0.02 to 0.10 in. (0.05 to 0.25 cm). For member thickness t = 0.02 in. (0.05 cm), the nodal lines for mode 2 (torsional) and mode 3 (bending) are quite clear. At t = 0.04 in. (0.10 cm), the two lines are migrating. At t = 0.06 in. (0.15 cm), each of the two modes have a mix of torsional and bending modes. At t = 0.08 in. (0.20 cm), modes 2 and 3 have switched. At t = 0.10 in. (0.25 cm), the new mode 2 (bending) and mode 3 (torsional) are quite discrete.

Flutter Analyses of Wing Box Models

The flutter predictions were checked for subsonic flow on the three- and six-bay wing boxes. The variables used were the same as those used to check the free-vibration frequencies. The unswept three-bay wing box was reported by Striz and Venkayya[16] to have a flutter velocity of 866 ft/s (264 m/s), at an altitude of 10,000 ft (3048 m), and a flight Mach number of 0.5566. The aerodynamic theory used for this prediction was the doublet-lattice method. Hemmig et al.[23] compared the aerodynamics approximated by the doublet-lattice method to

that by the linear strip theory and reported that the "difference between the flutter speeds computed by these two procedures is approximately 20%, and strip theory is conservative in that it predicts a lower speed." In this study, the frequency coalescence method with linear strip theory yielded the flutter speed to be 686 ft/s (209 m/s), which is approximately 20% on the conservative side. Under the same flight conditions, the divergence speed of a wing swept forward 30-deg with six bays was reported to be 515 ft/s (157 m/s).[13] In this study, the divergence speed of such a wing was found to be 525 ft/s (160 m/s). The change in flutter and divergence speeds with sweep in the subsonic regime matched the general trends reported by Bisplinghoff et al.[24]

Supersonic aerodynamics were modeled using a first-order high Mach number approximation to the linear potential flow theory with damping terms neglected,[17] the aerodynamic center located at the half chord. The conditions were assumed to be flight at Mach 2.0, at an altitude of 20,000 ft (6096 m), with the wing swept back at an angle of 30 deg with respect to the freestream.

To study the trends of flutter behavior, the thicknesses of the skins, webs, and ribs were varied for several cross-sectional areas of the spar caps and vertical posts, ranging from 0.5 to 1.5 in.^{2} (3.2 to 9.7 cm^2). These trends were studied for both a wing box with and without nonstructural masses, identical to those studied for free vibration trends. The flutter velocities for both cases are presented in Fig. 8, for easy comparison.

For the wing box without nonstructural masses, the mode of flutter involves the first torsion and second bending frequencies. The thickness value at which the frequencies of these two modes cross is worthy of special mention. At this crossing point, the frequency for the first torsional mode and that of the second bending mode are the same at zero freestream velocity, or zero flutter speed. The flutter velocity is zero at a skin, web, and rib thickness of 0.130 in. (0.32 cm) for the spar cap and vertical post cross-sectional area of 1.0 in.^{2} (6.5 cm^2), which corresponds to that reported earlier for the free-vibration analysis. Increasing the spar cap and vertical post cross-sectional areas moves this crossing point to higher skin, web, and rib thicknesses, whereas decreasing the member areas moves this crossing point to lower member thickness values.

Flutter behavior of the wing box is changed with the addition of nonstructural mass to the rear spar. For example, there is a significant drop in flutter speed at a skin, web, and rib thickness of 0.054 in. (0.137 cm) for the spar cap and vertical post cross-sectional area of 1.0 in.^{2} (6.5 cm^2). This drop in flutter velocity is a result of the switching from mode 1 and mode 2 coalescence (left-hand side of the curve) to mode 2 and mode 3 coalescence (right-hand side of the curve). As demonstrated in Fig. 8, adding the nonstructural masses to the rear spars, which is a more realistic model, has an effect of eliminating those zero-value cusps of the flutter curves for the wing box without nonstructural masses, moving the flutter curves to higher values with the bottom envelope values ranging from 600 to 900 ft/s (183 to 274 m/s). Increasing the spar cap and vertical post cross-sectional areas moves this switching point to higher skin, web, and rib thicknesses, whereas decreasing the member areas moves this switching point to lower member thickness values.

Flutter Control of Wing Box Models

The control of the wing box was implemented by adding piezoelectric elements and feeding back the modal gain that produces the desired free vibration frequency. The modal amplitudes were assumed to be observable to the controller; however, sensory actuators, such as PVDF would be required in an actual system. To achieve the amplitudes of deflection required by the wing box, the piezoelectric actuators were assumed to have twice the thickness of the skins, webs, and ribs. When the piezoelectric strips were added as shown in Fig. 3, it was assumed that the resulted additional stiffnesses and masses were too small to affect the frequencies as compared to the effect caused by the stresses induced by the strips.

To study the trends of controlling flutter, the skin, web, and rib thicknesses were varied for several controlled values of the natural modal frequency. The spar cap and vertical post cross-sectional areas were held at a constant value of 1.0 in.^{2} (6.5 cm^2), whereas the natural frequencies were modified ranging from −10% to +10% of the uncontrolled frequency. The controlled flutter velocity trends were studied for a wing box with and without nonstructural masses. These trends for both cases are presented in Fig. 9, for easy comparison.

For the wing box without nonstructural masses, the similarities between these results caused by frequency control and those caused by changes in the spar cap and vertical post cross-sectional areas shown in Fig. 8 are evident. It is noted that for 0% torsional frequency change, the pattern of the curve is identical to that shown in Fig. 8 with the spar cap and post

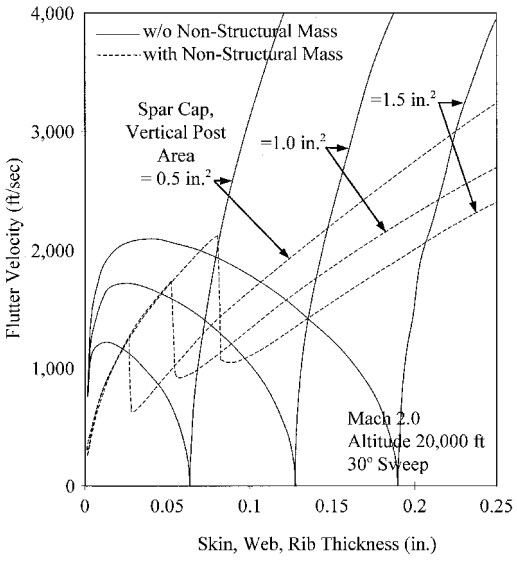

Fig. 8 Effect of skin, web, and rib thickness on flutter speed for specified spar cap and post cross-sectional areas of wing box with and without nonstructural masses.

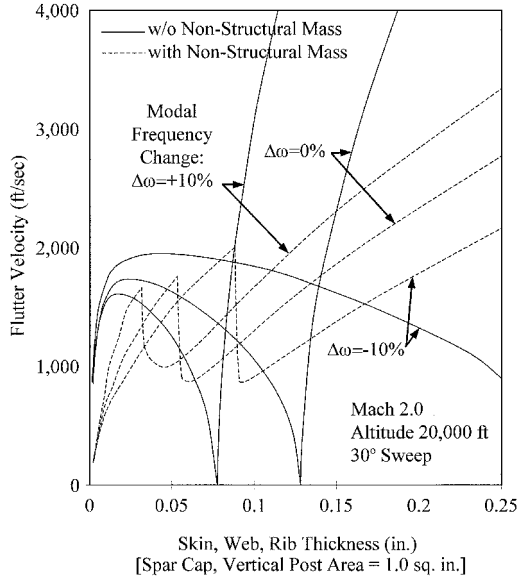

Fig. 9 Effect of skin, web, and rib thickness on flutter speed with modal frequency change of wing box with and without nonstructural masses.

Table 2 Comparison of design weights for wing box without nonstructural masses

Skin, web, rib thicknesses, in.	Spar cap, vertical post areas, in.^{2}	Frequency change, $\Delta\omega_2$, %	Wing box design weight, lb
0.15	1.0	+0	222
0.09	1.0	+10	243
0.06	1.0	−21 or +54	174
0.06	2.15	+0	231

cross-sectional area of 1.0 in.^{2} (6.5 cm^2). Lowering the torsional frequency is equivalent to increasing the spar cap and vertical post area that moves the crossing point to a higher skin, web, and rib thickness. Raising the torsional frequency is equivalent to lowering the member areas that moves the crossing point to higher member thickness values.

Control of the wing box with nonstructural masses distributed on the rear spar is complicated because of the control and aerodynamic coupled terms in Eqs. (20) and (21). To be consistent with the previous analyses, the nonstructural masses were again assumed to be equal to the mass of the original box structure. Because of the modal coupling, any one or more of the frequencies can be changed with appropriate feedback. The effect because of the variation of skin, web, and rib thickness, with spar cap and vertical post cross-sectional areas held at a constant value of 1.0 in.^{2} (6.5 cm^2), for the modified mode 3 frequency ranging from −10% to +10%, are presented in Fig. 9. It is noted that for 0% mode 3 frequency change, the pattern of the curve is identical to that shown in Fig. 8 with a spar cap and post cross-sectional area of 1.0 in.^{2} (6.5 cm^2). Changing the mode 3 frequencies results in flutter curves of the same patterns as those shown in Fig. 9.

Weight Comparisons for Controlled Wing Boxes

The requirement for minimum flutter speeds and for structural strength because of static equivalent lift load must be met by any design choice of skin, web, and rib thicknesses, and the spar cap and vertical post areas. An alternative approach is to select these variables to meet the strength requirement and to implement control devices to meet the flutter requirement. The weight of the design could become the deciding factor when comparing the two choices. The spar caps are assumed to primarily carry the bending stress of the static equivalent lift load. The spar cap area, which is of sufficient size to meet margin of safety requirements, was assumed to be 1.0 in.^{2} (6.5 cm^2) in this example. The flutter requirement for flight at Mach 2.0 and an altitude of 20,000 ft was assumed to be 2500 ft/s (762 m/s), corresponding to Mach 2.2, for this example.

For the wing box without distributed nonstructural masses, the flutter requirements can be met for a skin, web, and rib thickness of 0.15 in. (0.38 cm) as shown in Fig. 9. The wing box with piezoelectric actuators increasing the torsional frequency by 10% would meet the same flutter requirements at a skin, web, and rib thickness of 0.09 in. (0.23 cm) as shown in Fig. 9. The wing box with piezoelectric actuators weighs 243 lb (110 kg), whereas the weight of the wing box with the thicker skins, webs, and ribs is 222 lb (101 kg).

For the wing box with distributed nonstructural masses, the flutter requirements can be met for a skin, web, and rib thickness of 0.23 in. (0.58 cm) as shown in Fig. 9. The piezoelectric actuators increasing the third mode frequency by 10% would meet the flutter requirement at a thickness of 0.17 in. (0.43 cm) as shown in Fig. 9. The weight of the wing box with piezoelectric actuators is 353 lb (160 kg), whereas the weight of the wing box with thicker skins, webs, and ribs is 331 lb (150 kg). There is a weight penalty associated with the actuators because the decrease in skin, web, and rib thickness is small compared with the relative size of the piezoelectric actuators necessary to implement the frequency changes.

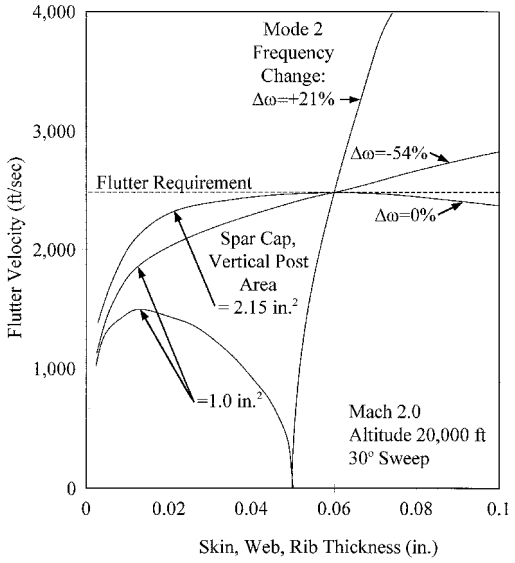

Fig. 10 Effect of spar cap and vertical post cross-sectional area and second-mode frequency change to meet flutter requirement of wing box without nonstructural masses.

For all cases, the trends show that for larger spar cap and vertical post areas, there is the possibility of meeting the flutter requirements at lower skin, web, and rib thicknesses. To elaborate on the advantage of using piezoelectric actuators for weight saving on the wing box without attached nonstructural masses, Fig. 10 is shown. It is seen that for skin, web, and rib thicknesses of 0.06 in. (0.15 cm), the flutter speed limitation of 2500 ft/s (762 m/s) can be met by decreasing the torsional frequency of the wing box by 54%, or increasing the torsional frequency of the wing box by 21%. It is emphasized that the piezoelectric strips in each cell are assumed to be sufficient in size to realistically achieve the high percentage changes required. Without piezoelectric actuators, to achieve this flutter requirement, a spar cap and vertical post cross-sectional area of 2.15 in.^{2} (13.9 cm^2) is needed. The weight of the wing box with piezoelectric actuators is 174 lb (78.9 kg), whereas the weight of the wing box with larger spar caps and vertical posts is 231 lb (105 kg). For convenience, a comparison of the resultant weights for the design of the wing box without nonstructural masses is included in Table 2.

The wing box with attached nonstructural masses can meet the flutter requirement of 2500 ft/s (762 m/s) at a skin, web, and rib thickness of 0.11 in. (0.28 cm) by using the piezoelectric actuators to increase the third mode frequency by 36%, as shown in Fig. 11. It is emphasized that the piezoelectric strips in each cell are assumed to be sufficient in size to realistically achieve the high percentage changes required. This requirement can also be met by a wing box with a spar cap and vertical post cross-sectional area of 2.15 in.^{2} (13.9 cm^2). The weight of the wing box with piezoelectric actuators is 255 lb (116 kg), whereas the weight of the wing box with larger spar caps and vertical posts is 286 lb (130 kg). For convenience, a comparison of the resultant weights for the design of the wing box with nonstructural masses is included in Table 3.

Table 3 Comparison of design weights for wing box with nonstructural masses

Skin, web, rib thicknesss, in.	Spar cap, vertical post areas, in.^{2}	Frequency change, $\Delta\omega_3$, %	Wing box design weight, lb
0.23	1.0	+0	331
0.17	1.0	+10	353
0.11	1.0	+36	255
0.11	2.15	+0	286

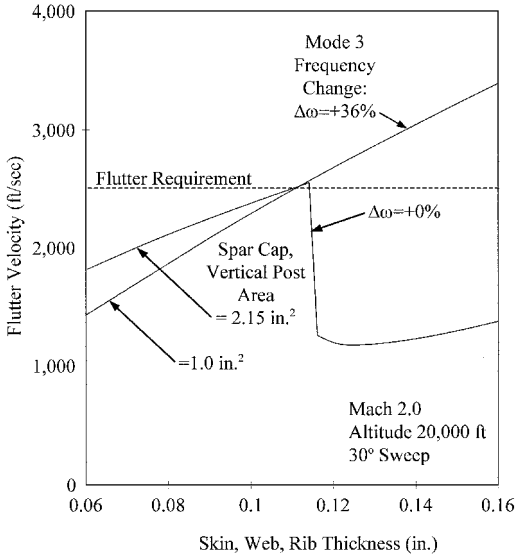

Fig. 11 Effect of spar cap and vertical post cross-sectional area and third-mode frequency change to meet flutter requirement of wing box with nonstructural masses.

Concluding Remarks

The control of flutter of a wing box using piezoelectric actuators has been presented. The free-vibration frequencies were changed by the piezoelectric actuators to increase the flutter speed caused by changed mode coalescence. The frequencies and modes can be modified by changing the design variables or using piezoelectric actuators. The examples indicated that the required flutter velocity of a wing box can be met by the addition of piezoelectric actuators in addition to changing the design variables. The examples further demonstrated that, for the cases and parameters chosen, noticeable reductions in the weight of the wing boxes without nonstructural masses can be achieved by the addition of piezoelectric actuators.

It is a logical next step to apply multi-input/multi-output control to change the free-vibration characteristics and to increase the flutter speed while achieving weight savings. Another logical next step is to perform an optimization study for a wider range of wing box designs to draw more concrete conclusions on and provide more insight to the concept of using piezoelectric actuators. The basic method is applicable to more complex built-up wing structures with more sophisticated aerodynamic calculation methods, and would be expected to show benefits to configurations in which the actuators are able to achieve larger deflections of twist and bending and, thus, increase the flutter speeds. Lastly, accurate sizing of the piezoelectric strips would be necessary in future research to ensure sufficent control to realistically achieve the high percentage changes required to the modal frequencies.

Discussion of Piezoelectric Actuator Implementation

The application of piezoelectric actuators for this study has been simplistic without regard to the additional effects caused by the weight of the sensors, control electronics, cabling, and additional power-generating capacity. Those effects may influence the frequencies, changes for nominal deflection magnitudes, and the flutter characteristics, thus requiring further study. The examples indicate that the mass of the piezoelectric actuators is not negligible as compared with the mass of the wing box. Although the trends may still be similar despite this additional consideration, the sizing of the adaptive systems with regard to both stiffness and mass must be included in a more precise integrated structure control design procedure.

Using piezoelectric material-based control systems that include components and performs functions of sensors, control electronics, cabling, and additional power-generating capacity would require the study of practical problems for application, such as detailed design and manufacturing. For example, the system must be reliable and robust to avoid possible malfunctions or dysfunctions caused by the dynamic characteristic and the very frequent off-and-on nature of the system. The solution would require future research using integrated approaches involving reliability studies, possible neuronetwork development, and other advanced technologies.

References

[1]Zeiler, T. A., and Weisshaar, T. A., "Integrated Aeroservoelastic Tailoring of Lifting Surfaces," *Journal of Aircraft*, Vol. 25, No. 1, 1988, pp. 76–83.

[2]Karpel, M., "Sensitivity Derivatives of Flutter Characteristics and Stability Margins for Aeroservoelastic Design," *Journal of Aircraft*, Vol. 27, No. 4, 1990, pp. 368–375.

[3]Noll, T. E., "Aeroservoelasticity," *Proceedings of the 31st Structures, Structural Dynamics, and Materials Conference* (Long Beach, CA), AIAA, Washington, DC, 1990, pp. 1560–1570.

[4]Wada, B. K., Fanson, J. I., and Crawley, E. F., "Adaptive Structures," *Mechanical Engineering*, Vol. 112, No. 11, 1990, pp. 41–46.

[5]Barrett, R., "Modeling Techniques and Design Principles of a Low Aspect Ratio Active Aeroservoelastic Wing," *Proceedings of the Smart Structures and Materials 1993: Smart Structures and Intelligent Systems Conference*, Vol. 1917, Society of Photo-Optical Instrumentation Engineers, 1993, pp. 107–118.

[6]Abdul-Wahed, M. N., and Weisshaar, T. A., "Active Tailoring of Adaptive Lifting Surfaces for Aeroelastic Applications," *Proceedings of the Smart Structures and Materials 1993: Smart Structures and Intelligent Systems Conference*, Vol. 1917, Society of Photo-Optical Instrumentation Engineers, 1993, pp. 72–83.

[7]De Luis, J., and Crawley, E. F., "Experimental Results of Active Control on a Prototype Intelligent Structure," *Proceedings of the 31st Structures, Structural Dynamics, and Materials Conference* (Long Beach, CA), AIAA, Washington, DC, 1990, pp. 2340–2350.

[8]Ehlers, S. M., and Weisshaar, T. A., "Static Aeroelastic Behavior of an Adaptive Laminated Piezoelectric Composite Wing," *Proceedings of the 31st Structures, Structural Dynamics, and Materials Conference* (Long Beach, CA), AIAA, Washington, DC, 1990, pp. 1611–1623.

[9]Lazarus, K. B., Crawley, E. F., and Bohlmann, J. D., "Static Aeroelastic Control Using Strain Actuated Adaptive Structures," *Proceedings of the 1st Joint U.S./Japan Conference on Adaptive Structures* (Maui, HI), 1990.

[10]Lazarus, K. B., Crawley, E. F., and Lin, C. Y., "Fundamental Mechanisms of Aeroelastic Control with Control Reversal and Strain Actuation," *Proceedings of the 32nd Structures, Structural Dynamics, and Materials Conference* (Baltimore, MD), AIAA, Washington, DC, 1991, pp. 1817–1830.

[11]Venkayya, V. B., and Tischler, V. A., "ANALYZE Analysis of Aerospace Structures with Membrane Elements," Air Force Flight Dynamics Lab., TR-78-170, Dec. 1978.

[12]Megson, T. H. G., "Stress Analysis of Aircraft Components," *Aircraft Structures*, 2nd ed., Halsted Press, New York, 1990, pp. 313–389.

[13]Bowman, K. B., Grandhi, R. V., and Eastep, F. E., "Structural

Optimization of Lifting Surfaces with Divergence and Control Reversal Constraint," *Structural Optimization*, Vol. 1, 1989, pp. 153–161.

[14]Rudisill, C. S., and Bhatia, K. G., "Optimization of Complex Structures to Satisfy Flutter Requirements," *AIAA Journal*, Vol. 9, No. 8, 1971, pp. 1487–1491.

[15]Rudisill, C. S., and Bhatia, K. G., "Second Derivatives of the Flutter Velocity and the Optimization of Aircraft Structures," *AIAA Journal*, Vol. 10, No. 12, 1972, pp. 1569–1572.

[16]Striz, A. G., and Venkayya, V. B., "Influence of Structural and Aerodynamic Modeling on Flutter Analysis," *Proceedings of the 31st Structures, Structural Dynamics, and Materials Conference* (Long Beach, CA), AIAA, Washington, DC, 1990, pp. 110–118.

[17]Kuethe, A. M., and Chow, C. Y., "Airfoils in Supersonic Flow," *Foundations of Aerodynamics*, Wiley, New York, 1987, pp. 278–286.

[18]Carter, R. E., "Transducer Elements," *Piezo Systems Product Catalog*, Piezo Systems, Inc., Cambridge, MA, 1990.

[19]Yang, T. Y., *Finite Element Structural Analysis*, Prentice–Hall, New Jersey, 1986.

[20]Beyer, W. H., "Cubic Equations," *CRC Standard Mathematical Tables and Formulae, 29th Edition*, CRC Press, Boca Raton, FL, 1991, p. 9.

[21]Skelton, R. E., "Pole Assignment," *Dynamic Systems Control*, Wiley, New York, 1988, pp. 318–321.

[22]Forster, E. E., "Flutter Control of Wing Boxes Using Piezoelectric Actuators," M.S. Thesis, Purdue Univ., West Lafayette, IN, Aug. 1994.

[23]Hemmig, F. G., Venkayya, V. B., Eastep, F. E., "Flutter Speed Degradation of Damaged, Optimized Flight Vehicles," AIAA Paper 79-0795, April 1979.

[24]Bisplinghoff, R. L., Ashley, H., and Halfman, R. L., "Introduction to Aeroelasticity," *Aeroelasticity*, Wiley, New York, 1955, pp. 1–14.